AMBIENT PRESSURE DRIFT REJECTION OF MODE-LOCALIZED RESONANT SENSORS

*Hemin Zhang, Jiming Zhong, Weizheng Yuan, Jing Yang, and Honglong Chang**
MOE Key Laboratory of Micro and Nano Systems for Aerospace,
Northwestern Polytechnical University, Xi'an, China

ABSTRACT

This paper experimentally demonstrates the ambient pressure drift rejection capability in the full measurement range of the mode-localized sensors. Based on a mode-localized resonant stiffness sensor, the experimental results show that the maximum measurement error of the amplitude ratio readout is ~2.74% whereas that of the frequency readout is ~21.63% with a pressure range of [2.6, 20] Pa. And the amplitude ratio based sensitivity is averagely ~1970.3 times higher than the frequency based sensitivity. It can be concluded that the mode-localized sensors can not only amplify the sensitivity but also reject the ambient pressure drift.

INTRODUCTION

Microelectromechanical system (MEMS) resonators are widely used for sensing applications. Natural frequency of the resonators will shift when the structural parameters such as stiffness and mass of the resonator are perturbed. In addition to such direct sensing, the MEMS resonator can also be used as the key element of sensors such as vibrational gyroscope [1]. In order to reduce the energy dissipation caused by air damping, the resonant sensors are always packaged in vacuum environment [2]. The quality factor can be improved by orders of magnitude after vacuum packaging. However, even the state of the art hermetic packaging techniques with getter inside cannot guarantee the operation pressure unchangeable in the whole lifetime of the sensors [3]. The small shift of the package pressure will cause the decrease of the quality factor and vibrational displacement. Furthermore, the small shift of the operation pressure will sometimes cause the shift of the frequency, which significantly influence the accuracy of the resonant sensors. Few methods are proved efficient enough to reject the pressure drift until the occurrence of the mode localization based sensors.

Mode localization in structure dynamics is usually described as that in a symmetrical weakly coupled resonators system, the application of a tiny symmetry-breaking perturbation to the structure will lead to the drastic vibrational energy confinement. The mode localization phenomenon has been used as a novel transduction scheme for enhancing the sensitivity of the resonant sensors by two or more orders of magnitude. Varieties of ultra-sensitive mass sensors [4-5], displacement sensors [6], stiffness sensors [7], accelerometers [8], tilt sensors [9], and electrometers [10] have been demonstrated. A marked feature of the WCRs-based sensors is that the output metric is not the frequency but the amplitude ratio or eigenstate. Because the output metric is the amplitude ratio, the mode localization based sensors have a good common mode rejection property to both temperature and pressure shift. However, no experimental data has solidly proved it. The validations in [11] were based on the responses of the resonators under only once structure perturbation (0.232N/m), which makes the conclusions not solid enough due to measurement uncertainties. In this paper, we will experimentally verify the capability by extending the structural parameter perturbations to the full range, and compare different output metrics including frequency, amplitude ratio and amplitude difference.

COMMON MODE REJECTION THEORY

Model of the WCRs

A simplified mass-spring-damper model of the WCRs is depicted in Figure 1. The mass and stiffness of the two resonators are assumed ideally symmetric, i.e. $m_1 = m_2 = m$ represents the effective mass of the resonator; $k_1 = k_2 = k$ represents the effective stiffness of the resonator; k_c is the coupling stiffness, Δk is the stiffness perturbation, x_1 and x_2 is the displacement of each mass.

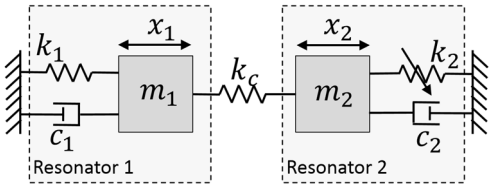

Figure 1. Schematic diagram of the mass-spring-damper model of a 2DoF WCRs.

The dynamic equations of the system without considering the damping can be given as:

$$\begin{bmatrix} m & 0 \\ 0 & m \end{bmatrix}\begin{bmatrix} \ddot{x}_1 \\ \ddot{x}_2 \end{bmatrix} + \begin{bmatrix} k+k_c & -k_c \\ -k_c & k+k_c+\Delta k \end{bmatrix}\begin{bmatrix} x_1 \\ x_2 \end{bmatrix} = 0 \tag{1}$$

The eigenfrequencies and amplitude ratios of the 2DoF system can be derived as:

$$\omega_i^2 = \frac{2k+\Delta k+2k_c \mp \sqrt{\Delta k^2+4k_c^2}}{2m} \tag{2}$$

$$u_i = \frac{x_{2i}}{x_{1i}} = \frac{\Delta k \pm \sqrt{\Delta k^2+4k_c^2}}{2k_c} \qquad i = 1,2 \tag{3}$$

where ω_i and u_i represents the resonant frequency and the amplitude ratio of the i^{th} mode, respectively. The relative shift or sensitivities of the resonant frequency and amplitude ratio can be written as:

$$S_\omega = \left|\frac{\omega_i - \omega_i^0}{\omega_i^0}\right| \cong \left|\frac{\Delta k}{2k}\right| \tag{4}$$

$$S_a = \left|\frac{u_i - u_i^0}{u_i^0}\right| \cong \left|\frac{\Delta k}{4k_c}\right| \qquad i = 1,2 \tag{5}$$

where S_ω and S_a represents the sensitivity based on the resonant frequency and amplitude ratio readouts, respectively. It can be deduced from (4) and (5) that the sensitivity based on amplitude ratio is about $k/2k_c$ times higher than that based on frequency shift.

By comparing the expressions of the amplitude ratio and frequency, it can be observed that the amplitude ratio based output metric is a dimensionless parameter while the frequency output is not. Therefore, any ambient pressure drift will affect both the numerator and denominator of the amplitude ratio output. The influence ambient pressure drift can thus inherently be cancelled, whereas the frequency output does not have this common mode rejection capability. This is very useful since most of the current package technology cannot ensure the long-time stability of the operation pressure.

DEVICE FABRACATION

In this paper, a 2-DoF weakly coupled resonators system is fabricated using the silicon on insulator process [12-13]. The device includes two double-ended-tuning-fork (DETF) resonators coupled by a mechanical beam. The device is actuated and sensed using capacitive transduction method. The sensing electrodes are placed at the center of the two tines of each DETF resonator. Therefore only the out-of-phase mode of the DETF can be detected. There are four tuning electrodes around the two resonators which are used for generating artificial stiffness perturbations to the coupled resonators. The SEM image of the device is shown in Figure 2.

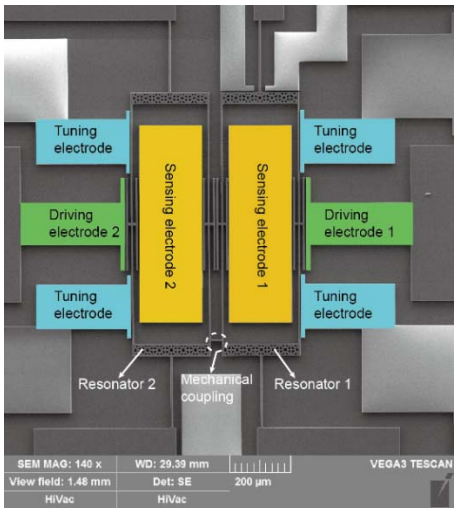

Figure 2. SEM image of the weakly coupled resonators.

The device was tested in a vacuum chamber where the operation pressure can be manually adjusted. The open-loop measurement setup is shown in Figure 3. A sweep AC signal from the signal generator was applied to the drive-port close to Resonator 2, and a DC bias voltage of 20V was applied on both DETFs to induce electrostatic actuation. The electric current signal from sense electrodes was sensed by a trans-impedance amplifier with a gain of 1MOhm, and observed on a dynamic signal analyzer. The feedthrough signal was cancelled using the method reported in [14]. The stiffness disorder of the WCRs caused by the fabrication tolerances can be compensated by tuning the DC voltage applied on the tune electrodes. The stiffness perturbation is calculated based on the formula $\Delta k = -\varepsilon A \cdot \Delta V^2/g^3$, where $\varepsilon = 8.85 \times 10^{-12}\ F/m$ is the permittivity of free space, $A = 9600\ \mu m^2$ is the effective cross-sectional area of the tuning capacitors, ΔV is the voltage difference between the tuning electrodes and the WCRs, and g is the capacitor gap of 3 μm.

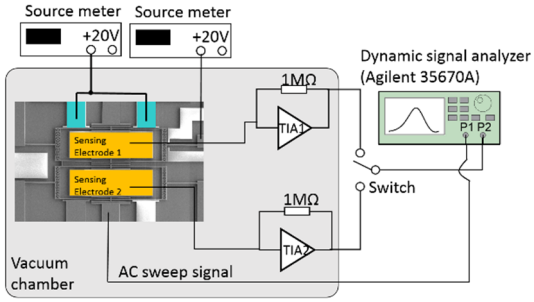

Figure 3. Experimental setup.

EXPERIMENTAL RESULTS

Responses of the coupled resonators

In order to verify the common mode rejection capability of the amplitude ratio readout, we recorded the magnitude-frequency responses of the two resonators under different operation pressures. The responses of Resonator 2 with the operation pressure of 2.6 Pa, 8.5 Pa and 20 Pa are shown in Figure 4.

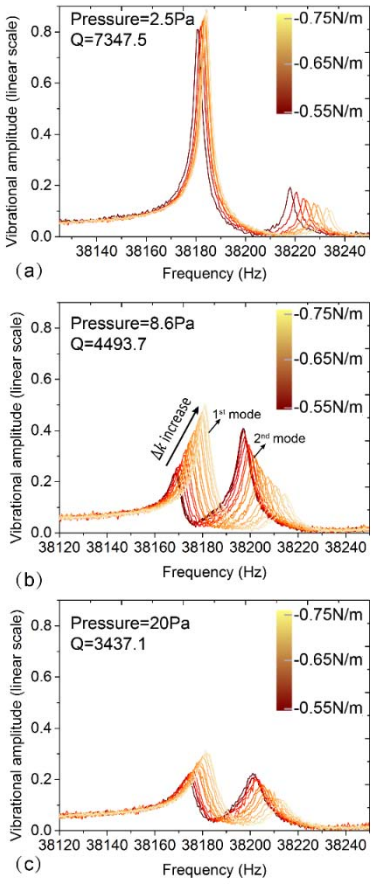

Figure 4. Frequency responses of Resonator 1 with different stiffness perturbations and operation pressures of 2.6 Pa (a), 8.5 Pa (b) and 20 Pa (c).

The quality factors under different operation pressures are 7347.5 (2.6 Pa), 4493.7 (8.5 Pa) and 3437.1 (20 Pa), respectively. It can be observed that with the increase of the operation pressure, the quality factor is decreased. Consequently, the vibrational amplitudes of Resonator 2 are decreased. Considering the responses with the operation pressure of 8.5 Pa, the vibrational amplitude of the 1st mode is increasing with the increase of the stiffness perturbation (Δk). In contrast, the amplitudes of the 2nd mode is decreasing with the increase of the stiffness perturbation (Δk).

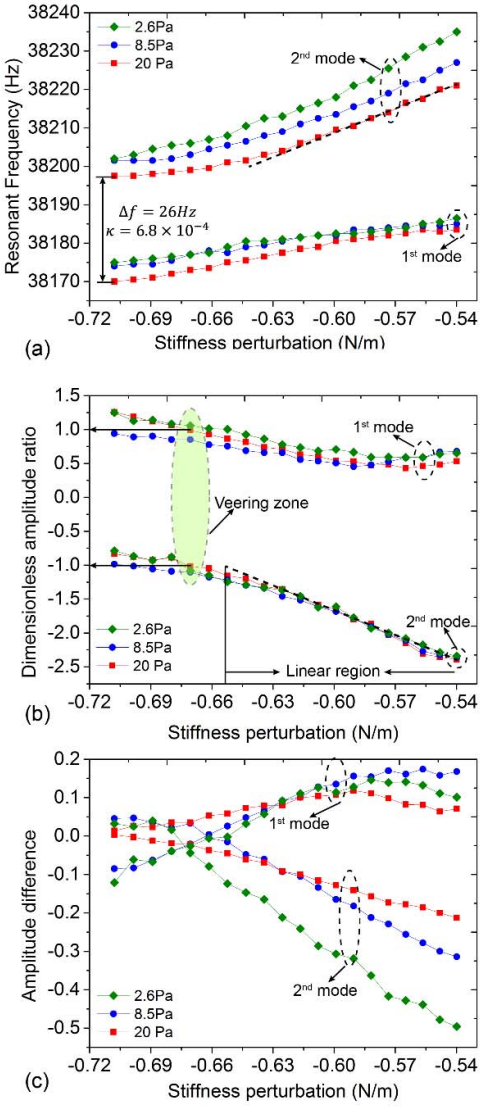

Figure 5. The resonant frequencies (a), amplitude ratios (b), and amplitude differences (c) as functions of the stiffness perturbations under different operation pressures.

Comparisons of the readouts

In order to compare the influences of the variations of the operation pressures to the frequency, amplitude ratio and amplitude difference readouts, we extracted the readout variations versus the stiffness perturbations under different operation pressures as shown in Figure 5. It can be seen from Figure 5(a) that the minimum frequency difference between the two modes is $\Delta f = 26$Hz, which indicates a coupling factor of $\kappa \sim 6.8 \times 10^{-4}$. With the increase of the stiffness perturbation, the resonant frequencies of the two modes gradually separate each other. And the resonant frequency of the 1st mode varies smaller than the 2nd mode by comparing the slopes of the frequency curves. Under different operation pressures, the frequency obviously performs different values. In contrast, as shown by Figure 5(b), the amplitude ratio readout of the 2nd mode is less affected by the variations of the operation pressure. Figure 5(c) shows the variations of the amplitude difference versus the stiffness perturbation under different operation pressures. It can be concluded by Figure 5 that the amplitude ratio readout demonstrates the best capability of rejecting the ambient pressure shift among the resonant frequency, amplitude ratio and amplitude difference readouts.

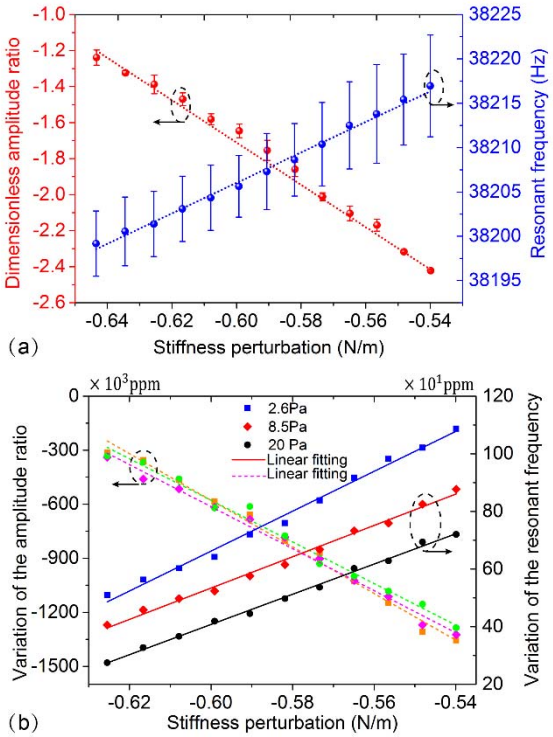

Figure 6. The mean values with error bars of the amplitude ratios and resonant frequecnies under different opearation pressures in the linear measurement range (a). The relative variations (sentivities) of the amplitude ratios and resonant frequencies as linear functions of the stiffness perturbations (b).

In order to compare the shift errors of the resonant frequency and amplitude ratio, we respectively calculated the mean values of the frequencies, amplitude ratios under different operation pressures. The error bars indicate the shift errors caused by the variations of the operation pressure. It can be observed that the maximum measurement error of the amplitude ratio readout due to the ambient pressure drift is ~2.74%, while that of the frequency readout is ~21.63% as shown in Figure 6(a).

The relative variations (sensitivities) of frequencies and amplitude ratios as linear functions of the stiffness perturbations are shown in Figure 6(b). It can be seen that the linear measurement range is [-0.63 N/m, -0.54 N/m]. And in the linear measurement range the amplitude ratio

based sensitivity is averagely ~1970.3 times higher than frequency based sensitivity.

CONCLUSIONS

In this paper, the ambient pressure drift rejection capability of the amplitude ratio readout of the mode-localized sensors is demonstrated in the full linear measurement range. This property is significantly useful since the operation pressure cannot be kept unchangeable in the whole lifetime of the resonant sensors using the current technologies.

ACKNOWLEDGMENTS

This work was supported by the National Natural Science Foundation of China under Grant 51575454.

REFERENCES

[1]. S. E. Alper, and T. Akin, "A single-crystal silicon symmetrical and decoupled MEMS gyroscope on an insulating substrate." *Journal of Microelectromechanical Systems*. vol. 14, no. 4, pp: 707-17, Aug. 2005.

[2]. A. A. Seshia, P. M. laniapan, T. A. Roessig, R. T. Howe, R. W. Gooch, T. R. Schimert, S. Montague, "A vacuum packaged surface micromachined resonant accelerometer," *Journal of Microelectromechanical Systems*, vol. 11, no. 6, pp. 784–793, Dec. 2002.

[3]. M. M. Torunbalci, S. E. Alper, T. Akin, "The advanced MEMS (aMEMS) process for fabricating wafer level vacuum packaged SOI-MEMS devices with embedded vertical feedthroughs." In 18th International Conference on Solid-State Sensors, Actuators and Microsystems (TRANSDUCERS'15) Jun 21-25. 2015, pp. 472-475.

[4]. M. Spletzer, A. Raman, A. Q. Wu, X. Xu, and R. Reifenberger. "Ultrasensitive mass sensing using mode localization in coupled microcantilevers". *Applied Physics Letters*, vol. 88, no. 25, pp. 254102, 2006.

[5]. P. Thiruvenkatanathan, J. Yan, J. Woodhouse, A. Aziz, and A. A. Seshia, " Ultrasensitive mode-localized mass sensor with electrically tunable parametric sensitivity," *Applied Physics Letters*, vol. 96, no. 8, pp. 081913, Feb. 2010.

[6]. P. Thiruvenkatanathan and A. A. Seshia, "Mode-localized displacement sensing," J. Microelectromech. Syst., vol. 21, no. 5, pp. 1016–1018, Oct. 2012.

[7]. C. Zhao, G. S. Wood, J. Xie, H. Chang, S. Pu, and M. Kraft. "A force sensor based on three weakly coupled resonators with ultrahigh sensitivity." *Sensors and Actuators A: Physical*, vol. 232, pp. 151-162, 2015.

[8]. H. Zhang, B. Li, W. Yuan, M. Kraft, and H. Chang, "An acceleration sensing method based on the mode localization of weakly coupled resonators," *Journal of Microelectromechanical Systems*, vol. 25, no. 2, pp. 286–296, Apr. 2016.

[9]. B. Li, H. Zhang, J. Zhong, and H. Chang, "A mode localization based resonant MEMS tilt sensor with a linear measurement range of 360 ". In IEEE 29th International Conference on Micro Electro Mechanical Systems, Jan 22-26, 2016, pp. 938-941.

[10]. H. Zhang, J. Huang, W. Yuan, and H. Chang, "A High-Sensitivity Micromechanical Electrometer Based on Mode Localization of Two Degree-of-Freedom Weakly Coupled Resonators." *Journal of Microelectromechanical Systems*. vol.25, no.5, pp: 937, Oct. 2016.

[11]. P. Thiruvenkatanathan, J. Yan, A. A. Seshia, "Differential amplification of structural perturbations in weakly coupled MEMS resonators." *IEEE Transactions on Ultrasonics, Ferroelectrics, and Frequency Control*. vol.57, no.3, pp: 690-7. Mar. 2010.

[12]. J. Xie, Y. Hao, Q. Shen, H. Chang, and W. Yuan. "A dicing-free SOI process for MEMS devices based on the lag effect." *Journal of Micromechanics and Microengineering*, vol. 23, no. 12, pp: 125033, Nov. 2013.

[13]. Y. Hao, J. Xie, W. Yuan, H. Chang, "Dicing-free SOI process based on wet release technology." *IET Micro & Nano Letters*, vol. 11, no. 11, pp: 775-778, Oct. 2016.

[14]. H. Zhang, W. Yuan, Y. Hao, and H. Chang, "Influences of the feedthrough capacitance on the frequency synchronization of the weakly coupled resonators", *IEEE Sensors Journal*, vol. 15, no. 11, pp. 6081-6088, Nov. 2015.

CONTACT

*Honglong Chang, changhl@nwpu.edu.cn